Sustainable Energy, Grids and Networks 39 (2024) 101491

Contents lists available at ScienceDirect

Sustainable Energy, Grids and Networks

journal homepage: www.elsevier.com/locate/segan

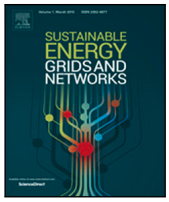

Dynamical heterogeneity and universality of power-grids

Bálint Hartmann [a,*], Géza Ódor [b], István Papp [b], Kristóf Benedek [c], Shengfeng Deng [d,b], Jeffrey Kelling [e,f]

[a] Institute of Energy Security and Environmental Safety, HUN-REN Centre for Energy Research, P.O. Box 49, H-1525 Budapest, Hungary
[b] Institute of Technical Physics and Materials Science, HUN-REN Centre for Energy Research, P.O. Box 49, H-1525 Budapest, Hungary
[c] Budapest University of Technology and Economics, Műegyetem rkp. 3, H-1111 Budapest, Hungary
[d] School of Physics and Information Technology, Shaanxi Normal University, Xi'an 710119, China
[e] Faculty of Natural Sciences, Chemnitz University of Technology, Straße der Nationen 62, 09111 Chemnitz, Germany
[f] Institute of Radiation Physics, Helmholtz-Zentrum Dresden-Rossendorf, P.O. Box 51 01 19, 01314 Dresden, Germany

ARTICLE INFO

Keywords:
Heterogeneity
Universality
Power system dynamics
Frequency
Community
Chimera

ABSTRACT

Electric power systems during transient states are extensively investigated using variations of the Kuramoto model to analyze their dynamic behavior. However, the majority of current models fail to capture the physics of power flows and the heterogeneity of the grids under study. This study addresses this gap by comparing the levels of heterogeneity in continent-sized power grids in Europe and North America to reveal the underlying universality and heterogeneity of grid frequencies, electrical parameters, and topological structures. Empirical data analysis of grid frequencies from the Hungarian grid indicates that q-Gaussian distributions best fit simulations, with spatio-temporally correlated noise evident in the frequency spectrum. Comparing European and North American power grids reveals that employing homogeneous transmission capacities to represent power lines can lead to misleading results on stability, and nodal behavior is heterogeneous. Community structures of the continent-sized grids are detected, demonstrating that Chimera states are more likely to occur when studying only subsystems. A topographical analysis of the grids is presented to assist in selecting such subsystems. Finally, synchronization calculations are provided to illustrate the occurrence of Chimera states. The findings underscore the necessity of heterogeneous grid models for dynamic stability analysis of power systems.

1. Introduction

Electric power systems under transients are often studied using variations [1–4] of the Kuramoto-model [5]. A notable shortcoming of this approach is that it relies on simplified models of the grid under study, including its infrastructural properties (topological and topographical structure, electrical parameters) and its behavior (volume of supply and demand at each node, spatio-temporal correlations), which may lead to qualitatively wrong results [6]. While agreeing that researchers are forced to make simplifications mainly because open data sources are rare and incomplete, bridging this gap is inevitable to effectively transform theoretical results into practice.

For this reason, the present paper focuses on completing the grid datasets using experience from the domain of power systems. Another goal is to use this process to deepen the understanding of dynamical heterogeneity and universality in power grids, continuing the work presented in [7].

Cascade failures in power grids occur when the failure of one component or subsystem causes a chain reaction of failures in other components or subsystems, ultimately leading to a widespread blackout or outage and disintegration of the network [8]. Historical data [9] and self-organized criticality (SOC) models [10] on direct current (DC) model simulation [11] have shown that blackout size distributions, measured by various quantities, energy, power, duration, can be described by fairly universal power-law (PL) tails [11,12], and SOC is expected to arise by the competition of trends in load demands weakening parts of the system and the responses to blackouts strengthening parts of the system [9]. To explain the scale-free behavior, its relation to the PL of city-size distributions has also been suggested [13].

Cascade failures in alternating current (AC) models have also been investigated [14–19]. Symmetry breaking (a situation where part of the oscillators, initially exhibiting symmetrical behavior, transition to a state where this symmetry is lost) in the network parameters, especially in the phase shifts between neighboring nodes, have been found

* Corresponding author.
E-mail addresses: hartmann.balint@ek.hun-ren.hu (B. Hartmann), odor@mfa.kfki.hu (G. Ódor).

https://doi.org/10.1016/j.segan.2024.101491
Received 20 December 2023; Received in revised form 2 July 2024; Accepted 26 July 2024
Available online 30 July 2024

List of symbols

α	Dissipation parameter
β	Power capacitance exponent of the generators
Γ	Resolution parameter of the community finding algorithm
γ	Decay exponent
κ	Kurtosis
$\langle k \rangle$	Average degree
Ω	Variance of frequencies
$\omega_i(t)$	Measured frequency of generator i
ω_i^0	Self frequency of generator i
$\sigma(x)$	Variance of quantity x
τ	Time lag
$\theta_i(t)$	Phase of oscillator i
AC	Alternating current
C	Auto correlation
C_{ij}	Capacitance of the power line between node i and j
d	Graph dimension
DC	Direct current
$ENTSO-E$	European Network of Transmission System Operators
$EU16$	European 2016 high-voltage power grid
$EU22$	European 2022 high-voltage power grid
f	Frequencies measured at substations
HOT	Highly optimized tolerance
HV	High voltage
I_i	Inertia of generator i
K	Coupling between the oscillators
k	Graph degree
LV	Low voltage
MV	Middle voltage
N	Number of nodes in the graph
$p(x)$	Probability density distribution of a quantity x
PDF	Probability density functions
PL	Power law
Q_i	Modularity of system i
R	Kuramoto phase order parameter
R_{ij}	Resistance of the power line between node i and j
SOC	Self-organized criticality
$T_{station}$	Super-statistical time scale of a given station
$US16$	United States 2016 high-voltage power grid
$USNW$	United States North-West high-voltage power grid
W_{ij}	Weight of the power line between node i and j
x	Admittance decay exponent
X_{ij}	Admittance of the power line between node i and j

to stabilize the synchronization [20]. Fine tuning of the asymmetry in the mass generators is essential, without this, local damage can cause fatal blackouts [21]. Our previous studies, which were based on solving the swing equations on different power-grids, arrived at different conclusions. While for a full high–middle–low voltage (HV–MV–LV) synthetic network a higher stability was found than on the 2-dimensional homogeneous lattice of same size [22], in the HV networks of Europe and Hungary, strong heterogeneity drastically reduces global synchronization [23]. An important and challenging question that remains is the determination of network topological effects and regions of enhanced stability, which can be obtained by symmetry breaking [24].

Very recently, PL blackout size distributions have been confirmed via AC modeling, using the numerical solution of the swing equations near the vicinity of the power-grid synchronization point [22,23,25]. For this, Gaussian distributed self-frequencies have been used, in general. The question arises whether the synchronization stability or the properties of cascade failures are altered by various heterogeneities (i.e. exponential or PL distribution of consumer and generator powers). Earlier it was found that these kinds of modifications in solutions of the swing equations lower the level of synchronization, but did not change the forms of failure cascade size distributions or the range of their occurrence in the control parameter space [23].

More generally, to explain PL electrical outage statistics, other mechanisms were proposed following the spectral analysis of large outage duration data sets. According to this solution, the observed auto-correlations in data for shorter durations imply a SOC mechanism of the competing maintenance supply and demand, leading to branching failure cascades [26]. SOC theory was introduced in the 1980s [10] to provide a possible explanation for the widespread occurrence of PL-s in nature [27]. For extended durations, the lack of such correlations suggested a highly optimized tolerance (HOT) mechanism [26].

While the previously mentioned topics are often examined using the variations [1,2] of the Kuramoto-model [5], notable shortcomings were highlighted recently, criticizing the simplicity of many solutions [28]. As a result, the physics of power flows and the heterogeneity and localization of generators and loads are not captured by the majority of current models.

In this paper we contribute to the deeper understanding of this aspect by (i) revealing the underlying heterogeneity of grid frequencies, topological structures and electrical parameters of real-world high-voltage grids, and (ii) comparing data of two widely used grid models to show that these heterogeneities show universal traces. We also provide a way to estimate missing admittances and graph edge weights for the variations of the Kuramoto model upon some assumptions. This method can help researchers create more realistic grid models, compared to the use of open-source and/or generative models (such as SciGRID, GridKit, PyPSA, OpenMod Initiative or the Open Power System Data models), which typically lack the level of detail necessary for case studies.

Finally, we provide an analysis of network communities in HV power-grids of Europe and north America. We shall point out that, contrary to the existing large heterogeneity, main features seem to be universal and may provide explanation for the frequent occurrences of power laws in the outage distributions. (The level of universality, of course, is just approximate, as various previous studies have found it [22,23,29,30].) Our results imply that PL emerges on continent sized networks, while sub-systems exhibit deviations from it. Here we go beyond static and graph theoretical analysis and provide a dynamical study by determining the graph communities and the synchronization in them via solving the swing equations. The role of communities, as strongly connected domains, can be very profound and may provide rare region effects, altering the dynamics of the system [31–33]. The modular structure can also enhance frustrated synchronization [34–37] and Chimera states [38,39], as demonstrated in the final part of our study. As far as frustrated synchronization is concerned, Kuramoto oscillators are expected to fully synchronize their phases and frequencies over time on homogeneous full graphs. In this respect, frustration refers to the phenomenon when the interactions hinder A fully synchronized state. This can be caused by conflicting interaction patterns, heterogeneous coupling strengths, or the inherent topology

of the network (like network modules). Meanwhile, the chimera state refers to the coexistence of synchronized and desynchronized regions in general, within the same system.

The remainder of the paper is organized as follows. Section 2 provides an overview of related literature, organized along the main aspects of the discussed shortcomings. Section 3 presents the results of the numerical modeling, and Section 4 discusses the main findings. Finally, conclusions are drawn in Section 5.

2. Heterogeneity and universality in empirical power-grid data

In this section, an analysis of various empirical data released concerning European power grids is presented. The non-Gaussian distributions obtained through this analysis underpin the necessity to perform numerical modeling by applying more sophisticated models, based on swing equations to be discussed below. Besides, we determine communities of the 2016 EU network by which the local synchronization analysis, started in Ref. [25], is extended.

The time evolution of power-grid synchronization is described by the swing equations [40], set up for mechanical elements (e.g. rotors in generators and motors) with inertia. It is formally equivalent to the second-order Kuramoto equation [1], for a network of N oscillators with phases $\theta_i(t)$. The second-order Kuramoto-model is one of the most successful mathematical models used to describe synchronization-related issues in power system analysis [2]. The field of its applications varies from transient stability analysis to topology design, as presented recently in [41]. Here a more specific form [22,42] is applied, which includes dimensionless electrical parametrization and approximations for unknown parameters:

$$\ddot{\theta}_i + \alpha\ \dot{\theta}_i = P_i + \frac{P_i^{max}}{I_i\ \omega_G} \sum_{j=1}^{N} W_{ij}\ \sin\left(\theta_j - \theta_i\right) . \tag{1}$$

In the above equation, α is the damping parameter, which describes the power dissipation, or instantaneous feedback [23]. $K := P_i^{max}$ is defined as a global control parameter, related to the maximum transmitted power between nodes. The inertia $I_i = I$ and the nominal generator frequency ω_G are kept constant in the lack of our knowledge. W_{ij} is the adjacency matrix of the network, which contains admittance elements, calculated from impedances to be described in Section 3.1. The constant external drive, denoted by $P_i := \omega_i^0$, which is proportional to the self-frequency of the ith oscillator, carrying a dimension of inverse squared time $[1/s^2]$, describes the power in/out of a given node. Thus, Eq. (1) is the swing equation (phases without amplitudes) of an AC power circuit. As is customary with the first-order Kuramoto model, the self-frequencies are drawn from a zero-centered Gaussian random variable, as rescaling invariance allows to gauge out the mean value in a rotating frame. For simplicity, one can assume that $\omega_i(0)$ is drawn from the same distribution as ω_i^0 and numerically set $\omega_i(0) = \omega_i^0$. In this study, the following parameter settings were used: the dissipation factor α is chosen to be equal to 0.4 to meet expectations for power grids, with the $[1/s]$ inverse time physical dimension assumption. Note, however that the massive Kuramoto Eq. (1) exhibits a rescaling invariance [25], thus the parameter values used can be changed and taken to be dimensionless.

The following subsections A-D separately discuss the state-of-the-art and our contributions in relation to four topics: grid frequency distributions, capacity distributions, topological and topographical structure of the grid, respectively.

2.1. Heterogeneity in grid frequency distributions

The Kuramoto equations show that the frequencies of the oscillators constitute an important variable to power-grid dynamics. Firstly, the nominal frequency ω_G may show slight spatial variation. Secondly, the measured frequency $\omega(t)$ will fluctuate in the vicinity of ω_G due to the system dynamics [43], despite the efforts to bring the system to synchronization.

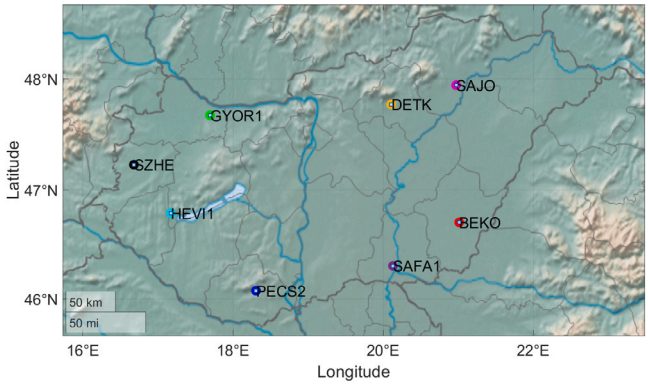

Fig. 1. Locations of frequency measurement sites used for the analysis. Abbreviations refer to 400 kV substations, as follows: BEKO — Békéscsaba, DETK — Detk, GYOR1 — Győr, HEVI1 — Hévíz, PECS2 — Pécs, SAFA1 — Sándorfalva, SAJO — Sajószöged, and SZHE — Szombathely.

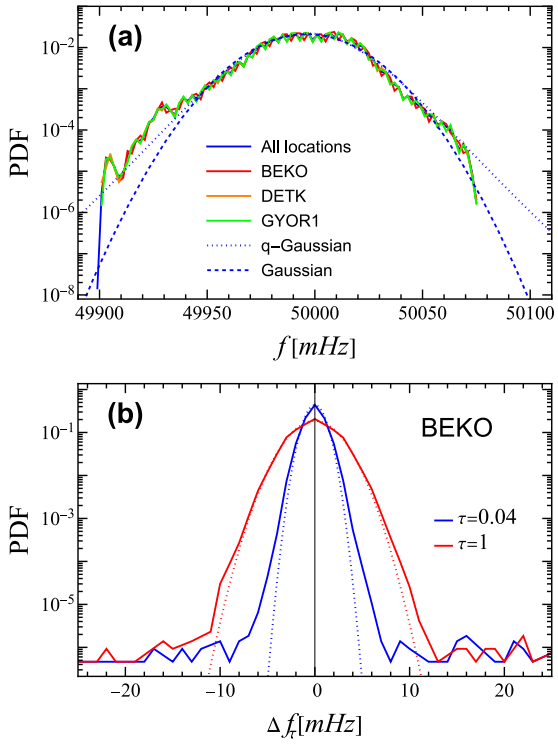

Fig. 2. Probability density functions (PDF) of (a) frequencies measured at different locations and of (b) increments of BEKO at time lags $\tau = 0.04$ s and $\tau = 1$ s. In (a), the Gaussian fit is $\mathcal{N}(49\,996.2601, 18.9679)$ and the q-Gaussian fit is given by the expression $\frac{0.0220}{\left(1+0.000\,179(49\,996.3-x)^2\right)^{9.274}}$ with $q \simeq 1.1078$. The dotted lines in (b) are the corresponding Gaussian distribution fits.

In the past decade and a half, various approaches have been employed in modeling frequencies within the Kuramoto equations [6]. The research community did not only search for more accurate representations, but they also examined the effect of frequency distributions on synchronization and stability. In their early work, Filatrella et al. [44] suggested that a bimodal distribution of frequencies is the most appropriate one for the power grid, a consideration which served as a basis for later studies. A different approach was presented by Olmi et al. [45], who used natural frequencies randomly distributed according to a Gaussian distribution, and by Pinto and Saa [46] and Taher et al. [47], who drew initial frequencies from uniform distributions.

It was shown in [48] that the addition of a stochastic noise and modeling random frequencies of distributed generation do not affect the forms of desynchronization distributions. Their results imply that heterogeneous networks have better performances than what homogeneous approximations could predict. In [7], the Gaussian self-frequencies were replaced by exponentially distributed ones. This change led to a drop in the steady state synchronization averages, but did not affect cascade size distributions.

Recently the focus of research was shifted to the analyses of frequency measurement data and their implication on synchronization. Wolff et al. [49] found that local frequency deviations from the nominal frequency show Gaussian nature for small deviations and an exponentially decaying tail part. In their papers [50–52], Rydin et al. conclude that histograms of frequency measurements are good indicators of how heavy-tailed the distributions are. It is shown that synchronously recorded frequency data exhibits very complex spatio-temporal behavior, and small fluctuations around the mean follow different types of super-statistics. A subsequent work [53] capitalizes on these experiences and proposes a Fokker–Planck equation to extend stochastic power-grid frequency models to handle non-Gaussian statistics as well. A different stochastic process, an Ornstein–Uhlenbeck process is suggested by [54] to model statistical properties (e.g. double-peaked probability density functions, heavy tails) of frequency measurements. Finally, Jacquoud et al. [55,56] show that non-Gaussian fluctuations of frequency decay with the distance from the source faster than Gaussian ones do, but such noise also propagates through the whole grid, resulting in voltage angle fluctuations resembling the same non-Gaussian distribution.

To demonstrate the variation and fluctuation of power-grid frequency, empirical frequency data were published, which were measured synchronously at eight different locations across Hungary within 24 h on Oct. 23 2022 [57]. The nominal synchronous frequency of the Hungarian Grid is 50 Hz and the recordings were taken at 8 sites at an interval of 0.02 s (see Fig. 1 for locations). As shown in Fig. 2(a), the bulk behavior of the frequency [denoted by $f(t)$ to distinguish it from $\omega(t)$ in the Kuramoto rotating frame] basically follows a Gaussian distribution. The only difference is that the tail parts are slightly heavier than in the Gaussian curve, which could be better fitted with a q-Gaussian curve with q very close to 1. Note that the q-Gaussian probability density function

$$p(x) = \frac{\sqrt{\beta}}{C_q} e_q^{-\beta x^2}, \ \beta = \frac{1}{2\sigma^2} \tag{2}$$

recovers the Gaussian distribution if $q \to 1$. Furthermore, for $q < 1$, $e_q^x = [\mathrm{ReLU}(1+(1-q)x)]^{\frac{1}{1-q}}$ is the q-exponential, where ReLU is the so-called rectified linear unit activation function, and C_q is the normalization factor for the distribution. (See Ref. [58] for a detailed account of this definition.) Due to the synchronization of the power system, frequency time series from different locations usually seem to be almost identical on a coarse time scale, regardless of the measured locations [59]. This phenomenon gives rise to an almost identical bulk distribution, which may be utilized as an initial condition for the Kuramoto equation (1).

However, on a short time scale of a few hundred milliseconds, frequencies fluctuate around the synchronous behavior, leading to distinct dynamics for each recording [60]. These fluctuations can be studied by the increments of frequencies [60,61]

$$\Delta f_\tau(t) = f(t+\tau) - f(t), \tag{3}$$

where τ is the incremental time lag. The increment of a time series is useful in that it eliminates the deterministic trends and focuses on the stochastic characteristics of the fluctuations on the shortest time scales. In contrast to the frequency distribution, Fig. 2(b) shows that the frequency increment distributions, here with the example for the BEKO case, are characterized by much heavier tails than those of Gaussian distributions (leptokurtic with kurtosis $\kappa > 3$). This non-Gaussian behavior suggests that the system is genuinely non-equilibrium, as power generation and consumption change over a long time scale, e.g. over one day. Then, similarly to the super-statistics of the overall energy distribution of a non-equilibrium system contained in a volume (which can be regarded as a superposition of Gibbs distributions pertaining to equilibrium states reached in small local cells [62]), it has been demonstrated that the observed non-Gaussian distribution for frequency increment may also be explained by super-statistics if one divides the increment time series into snippets [60]. Due to the relation between the frequency and its increments (3), the super-statistics of $\Delta f_\tau(t)$ may also be connected to the super-statistics of the frequency itself. The reason for this might be, as Ref. [62] showed, that the origin of q-Gaussian behavior in complex systems can be explained by a super-statistical framework, as manifested for the frequency. To demonstrate how stability analysis and related fields can benefit from the previous findings, we briefly present the main idea of super-statistics following Ref. [60], and the results for the Hungarian data-sets.

Fig. 2(b) showed that the Kurtosis of the whole frequency increment time series is larger than 3 (i.e. leptokurtic). If one looks at a shorter increment time series of time length δt, it should be expected that at a short enough intermediate time scale $\delta t = T$, local equilibrium characterized by a Gaussian distribution will be reached. For even shorter increment time series with $\delta t < T$, larger deviations from the mean do not have sufficient chances to occur, so the distribution is intrinsically platykurtic, characterized by thinner tails ($\kappa < 3$). In practice, one may slice the whole increment time series corresponding to the time lag τ into snippets of time duration δt and study their averaged kurtosis at this time scale δt:

$$\kappa_{\delta t}(\Delta f_\tau) = \left\langle \frac{\frac{1}{\delta t}\sum_{i=(j-1)\delta t+1}^{j\delta t} \Delta f_\tau^4(i)}{(\frac{1}{\delta t}\sum_{i=(j-1)\delta t+1}^{j\delta t} \Delta f_\tau^2(i))^2} \right\rangle_{\delta t}. \tag{4}$$

At an intermediate time scale $\delta t = T$ when $\kappa_{\delta t=T} = 3$, the snippets just resemble the local equilibrium cells of non-equilibrium thermal systems, only that the underlying equilibrium distribution is now assumed to be Gaussian. In accord with super-statistics [60,62], the frequency increment distribution can be expressed as superposed by a spectrum of Gaussian distributions:

$$p(\Delta f_\tau) = \int_0^\infty F(\beta) p_N\left(\Delta f_\tau|\beta\right) d\beta, \tag{5}$$

where $p_N(\Delta f_\tau|\beta) = \sqrt{\frac{\beta}{2\pi}} e^{-\frac{1}{2}\beta \Delta f_\tau^2}$. To properly separate different time scales, a caveat to note is that this super-statistics analysis is valid only if the super-statistical variation time scale T is much greater than the local relaxation time scale d, as strong auto-correlation will hinder the reaching of a local equilibrium. The time scale d can be determined by the auto-correlation function

$$C(t-t') = \left\langle (\Delta f_\tau(t) - \langle \Delta f_\tau \rangle)(\Delta f_\tau(t') - \langle \Delta f_\tau \rangle) \right\rangle \tag{6}$$

via $C(d) = e^{-1}C(0)$.

In Figs. 3(a) and (b), the kurtosis indeed shows a transition from $\kappa_{\delta t} < 3$ to $\kappa_{\delta t} > 3$ as δt increases, and for $\tau = 0.04$, $T \gg d$ is strictly held. Fig. 3(c) further shows the spectrum $\overline{F}(\beta) = F(\beta)/\max(F(\beta))$ with β values extracted from the inverse variance of the snippets at $\delta t = T$:

$$\beta_T(t) = \frac{1}{\langle \Delta f_\tau^2(t)\rangle_T - \langle \Delta f_\tau(t)\rangle_T^2}, \tag{7}$$

where the index T means that the averages are performed over snippets of length T. For $\tau = 0.04$ seconds, since $T \gg d$ holds, the spectra $\overline{F}(\beta)$-s span wide distributions and are distinct for recordings of different locations. When we increase the time lag to $\tau = 1$ second, T-s become only a few times larger than the corresponding d-s, and the spectra are much narrower.

Based on the analyzed measurements we conclude that

(i) a q-Gaussian is the best fit for the distribution of grid frequencies,

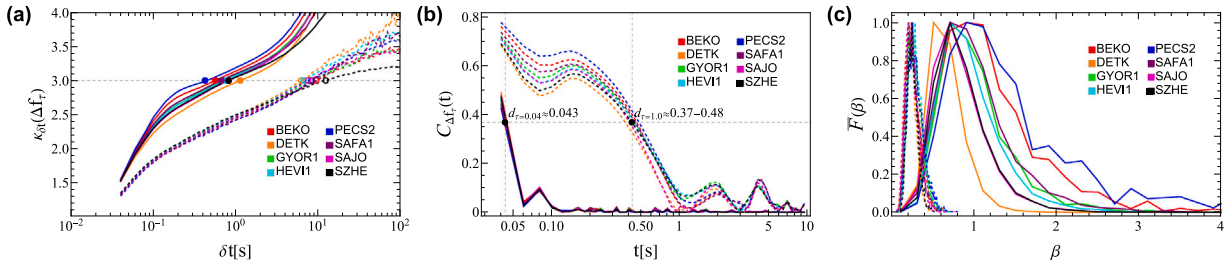

Fig. 3. (a) Snippet kurtosis, (b) connected auto-correlation functions, and (c) spectra of frequency increments of different locations at time lags $\tau = 0.04$ seconds (solid curves) and $\tau = 1$ second (dashed curves). In (a), the super-statistical time scales are $T_{\mathrm{BEKO}} = 0.562688$, $T_{\mathrm{DETK}} = 1.13538$, $T_{\mathrm{GYOR1}} = 0.680575$, $T_{\mathrm{HEVI1}} = 0.748079$, $T_{\mathrm{PECS2}} = 0.423406$, $T_{\mathrm{SAFA1}} = 0.668517$, $T_{\mathrm{SAJO}} = 0.821327$, and $T_{\mathrm{SZHE}} = 0.822878$ when $\tau = 0.04$, and are $T_{\mathrm{BEKO}} = 9.50441$, $T_{\mathrm{DETK}} = 6.21044$, $T_{\mathrm{GYOR1}} = 8.35081$, $T_{\mathrm{HEVI1}} = 6.68289$, $T_{\mathrm{PECS2}} = 8.2801$, $T_{\mathrm{SAFA1}} = 8.44334$, $T_{\mathrm{SAJO}} = 7.52667$, and $T_{\mathrm{SZHE}} = 12.4069$ when $\tau = 1$.

(ii) the frequency increment time series display spatial–temporal correlations. Hence, power system stability studies should extend their analysis beyond uncorrelated noise to correlated noise.

(iii) further research is necessary to examine whether fluctuation of grid frequency in simulations leads to super-statistical behavior.

2.2. Heterogeneity in capacity distributions

Representing the heterogeneous nature of the transmission infrastructure is typically done either by using the grid model of a country of synchronous area or by modifying the coupling strengths of the Kuramoto equation according to a pre-specified probabilistic distribution. In this section, a brief overview is provided for both aspects, along with addressing some limitations or deficiencies found in the existing literature.

Olmi et al. used the representations of the Italian [45] and the German [47] power grids, which were good examples of heterogeneous topologies; however, the coupling strength was assumed to be identical for all lines. Similarly, a uniform coupling strength, 1600 MW, representing the capacity of a 380 kV line was used in the examinations of Menck et al. [63]. Schäfer et al. [64] generated two homogeneous and a heterogeneous representation of the Turkish power grid, using the magnitude of power flows to represent the coupling strengths.

Real-world, heterogeneous grid topologies were used by Nishikawa and Motter [65], who showed that there is a non-trivial structure in the coupling among the generator nodes and that the coupling strength spans across many orders of magnitude. Large synthetic networks were generated with characteristics of real power grids exhibiting hierarchical modular structure, low clustering and topological dimensions, which resemble medium-distribution networks, to examine synchronization processes [48]. Kim et al. showed a heterogeneous distribution of load and generation in their paper [66], which were investigated under the condition of varying coupling strength, concluding that concentration of power generation at a single location is likely to increase vulnerability to perturbations. As a case study of the German power grid, they also reveal that the modular structure of the power grid does affect its vulnerability [67]. Ódor and Hartmann [7] concluded that too weak quenched heterogeneity of couplings among oscillators is not sufficient to observe power-law tailed distributed cascades. They also pointed out, that too strong heterogeneity destroys the synchronization of the system.

To demonstrate the nature of heterogeneity in terms of **power capacity**, the ENTSO-E 2016 data-set was analyzed, which includes information about the voltage level and the thermal power limit of the transmission lines. Using these two, the theoretical maximum transmittable power can be determined. The above-mentioned data was available for 8511 lines, of which 4024 were 220 kV lines, 592 were 275 kV lines and 3738 were 400 kV lines; these three groups represent the vast majority of infrastructural elements to be considered. As it is shown in Fig. 4, the capacity distribution of three selected voltage levels display rather different characteristics, with mean capacities at 254, 480 and 1144 MW for 220, 275 and 400 kV, respectively. The average power capacity of the lines in the ENTSO-E 2016 model, considering all voltage levels is 666.4 MW an atypical value for any widely used voltage level.

In many studies the generators/load capacities are assumed to be constant and are described by Gaussian centered ω_i-s or by some bimodal distributions. To demonstrate the nature of heterogeneity and universality in terms of **nodal behavior**, generation and load values of the ENTSO-E 2016 and the 2021 US [68] data set are presented. (It has to be noted that these values represent a single, but characteristic operational point of the European and the US power system.) As one can see in Figs. 5 and 6, nodal behavior is far from being uniform and can be approximated by stretched exponential functions in wide MW ranges of the form

$$p(k) \propto \exp(-(k/B)^{\beta}) \,, \tag{8}$$

with similar exponents. But PL-s can also be fitted for rather wide power ranges, with different success and exponents. The generator distributions stretch to MW values higher than the load distributions and exhibit a sharp cutoff if we assume PL-s. The fitting of Pareto-like functions was not successful.

Based on the analysis of the European and US grid datasets we find that

(i) using a homogeneous capacity in studies could easily under- or overestimate the strength of the coupling between nodes, thus giving misleading results on stability;

(ii) distribution of generation and load nodes is far from being uniform, thus heterogeneous modeling of capacities is necessary.

2.3. Topological structure of the European and North American HV powergrids

As a standard characterization of networks, first the comparison of the **degree distributions** of the EU16 (European 2016) [69], US16 (North-American 2016) [69], EU22 (European 2022) [70], USNW (US North-West) [71] graphs are shown. Fig. 7 summarizes the results, obtained using logarithmic binning for the different grids.

The PDFs look rather similar, with the outlier EU22 case, which decays almost as fast as the USNW, which is just the subset of the US power-grid: the standard North American HV grid, used in many graph theoretical papers [71]. Whether exponential, power-law or mixed distributions are the best fits to cumulative probability distributions of node degrees is still somewhat controversial, as pointed out in [72]. Here results of the common census for HV networks are presented, fitting with exponential functions in the following form:

$$p(k) \propto \exp(-\gamma k) \,. \tag{9}$$

Note that other authors [29,73] often consider the cumulative distributions $p(k > K)$ to achieve lower fluctuations in the tails. As Fig. 7 shows, the γ parameters are rather close to the value $\gamma = 0.5$. The γ parameters are summarized in Table 2.

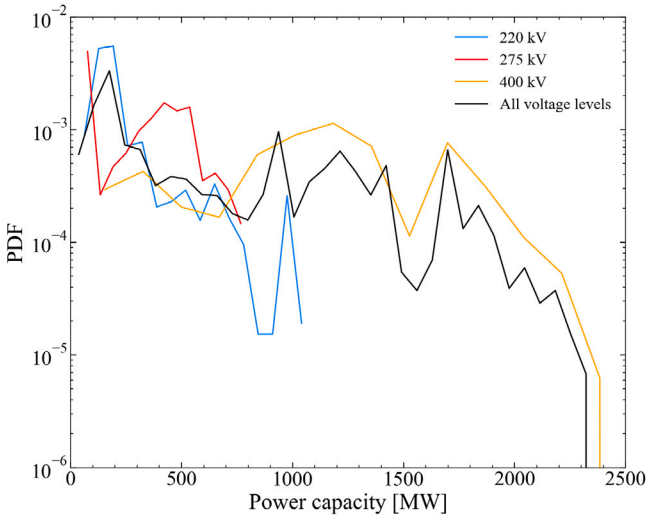

Fig. 4. Distribution of thermal power limits of transmission lines included in the ENTSO-E 2016 database. Contributions of 220, 275 and 400 kV lines are highlighted as the biggest populations. The distribution does not reflect the combined length of voltage levels, only the number of lines.

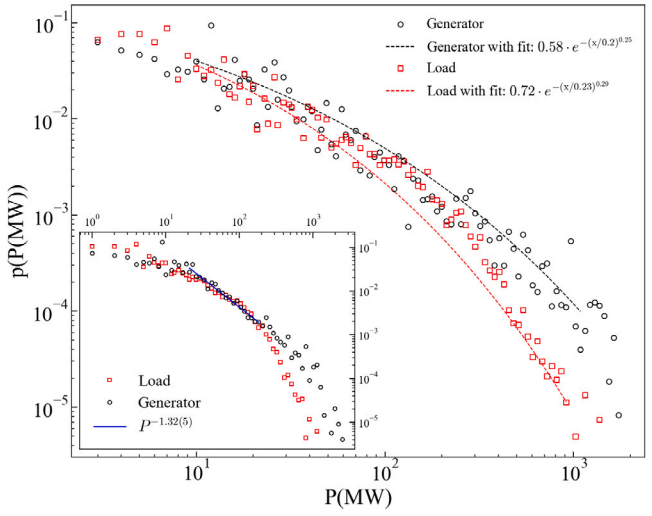

Fig. 5. Distribution of nodal generations and loads of the ENTSO-E 2016 database. Power-law fits were applied to the [20–300] MW range in the inset figure. The exponents of the fits are: $y = 1.16(5)$ both for generation and load curves, respectively. The load data shows an earlier size cutoff, which is an important characteristic of traditional power systems, where energy is produced in a centralized manner by large power plants to increase efficiency, and energy is consumed in a distributed manner. The main figure shows the same data, with stretched exponential fits, according to Eq. (8) in the range [10–1000] MW.

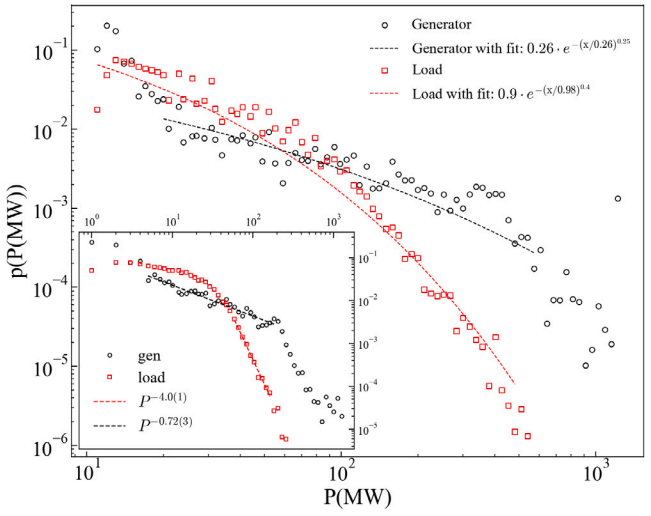

Fig. 6. Distribution of nodal generations and loads of the 2021 US [68] database. Inset: different power-law fits were applied to the [5–200] MW for generators and [50–200] MW for loads. The load data shows an earlier size cutoff as for the European case. The main figure shows the same data with stretched exponential fit according to Eq. (8) in the range [20–500] MW.

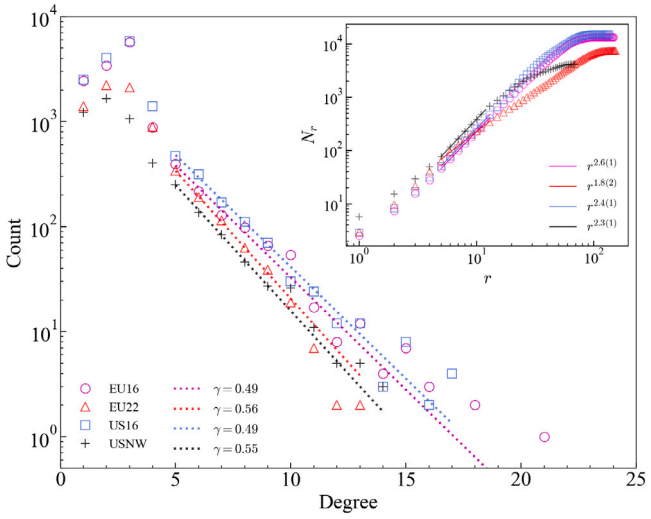

Fig. 7. Basic graph invariants of the power grids investigated. Main plot: degree distribution, using logarithmic binning. Exponential fits of form Eq. (9) for $5 < k < 15$ resulted in similar γ values. In the inset, the graph dimension analysis results of these graphs are presented. PL fits of form Eq. (11) for $5 < r < 20$ provide similar d-s, except for the EU22 case, plotted by red triangles. (For interpretation of the references to color in this figure legend, the reader is referred to the web version of this article.)

In what follows, the topological heterogeneity of power-grid networks are tested through their **community structures** [74,75]. Communities in networks are usually groups of nodes that are more densely connected to each other than to the rest of the network and as such, they can be considered as unique patterns of the heterogeneity that characterizes the topology. One might intuitively assume that a network with a greater number of communities exhibits increased diversity, potentially resulting in weaker synchronization on a global level. However, due to the size dependence of R in the case of the crossover synchronization transition of the second order Kuramoto model, small communities synchronize at smaller couplings K [76], leading to Chimera states, as shown in Section 3.2.

We used openly available data for the power grid network from ENTSO EU transmission data set from 2016 and from 2022, combined with OpenStreetMap for power-line identifications. For detecting the community structure, the hierarchical Louvain [77] method was chosen due to its speed and scalability, as this algorithm runs almost in linear time on sparse graphs, like power grids. The Louvain algorithm is based on modularity optimization. For finding communities on a higher level, the Leiden [78] algorithm optimizing an extended modularity quotient with a resolution parameter was also applied. The modularity quotient of a network is defined by [79]

$$Q = \frac{1}{N\langle k\rangle} \sum_{ij} \left(A_{ij} - \Gamma \frac{k_i k_j}{N\langle k\rangle} \right) \delta(g_i, g_j), \tag{10}$$

where A_{ij} is the adjacency matrix, k_i, k_j are the degrees of nodes i and j, and $\delta(g_i, g_j)$ is 1 when i and j were found to be in the same community, or 0 otherwise. Γ is the resolution parameter that allows

Table 1
Community sizes and average degrees for different data-sets, for the resolution $\Gamma = 10^{-4}$. Sizes are referred to here as number of nodes in the respecting community. These structures correspond to the maps plotted on Figs. 9, 11, 12.

Community	Size (EU22)	$\langle k \rangle$ (EU22)	Size (EU16)	$\langle k \rangle$ (EU16)	Size (US16)	$\langle k \rangle$ (US16)
1	924	2.72	4285	2.83	3511	2.79
2	479	2.70	2526	2.66	2829	2.98
3	2016	2.84	1527	2.67	1640	2.72
4	698	3.06	1461	2.72	1484	2.69
5	595	2.94	1455	2.69	1396	2.93
6	1059	2.66	966	2.77	1165	2.58
7	1237	2.68	638	2.57	768	2.97
8	16	2.81	289	2.06	710	2.57
9	332	2.18	277	2.99	673	2.70
10	55	2.74	26	3.07	390	2.84
11	–	–	22	3.31	230	2.43
12	–	–	6	2.66	194	2.69

a more generalized community detection, merging together smaller communities.

Community detection algorithms based on modularity optimization are believed to get the closest to the true modular properties of the network. With $\Gamma = 1$, ≈ 425 communities were found, with maximum modularity score of $Q_{EU16} = 0.92724$. For reference, the results were compared with the 2016 USA network (obtained similarly), which has larger number of nodes in the giant component: 14 990 connected by 20 880 links. At $\Gamma = 1$ for USA, 460 communities gave high modularity score of $Q_{US16} = 0.92525$. This result is in concordance with the previously calculated modularity [25]. To obtain community structures similar to the real TSO areas of typically 10–12 domains, was rerun with $\Gamma < 1$. Good agreement has been found as discussed in Section 2.4 and shown on Figs. 8, 9, 10, 11.

We could also compare the communities of 2016 power-grids with that of a 2022 EU one. This network, at first glance, seemed to be multiple connected, containing sub-networks of different voltage levels. After the unification at nodes with the same node IDs, a graph was obtained, which seems to be incomplete in several ways. It does not contain nodes with $k = 27$ as the 2016 one, but $k_{max} = 14$. Furthermore, looking at the node degree and edge length distributions, it appears that links are missing from the middle k region. More importantly, the node number of the largest component is just $N_{EU22} = 7.411$, contrary to the $N_{EU16} = 13.478$, even though the graphical map shows nodes in North Africa as well as in the Middle East, see Fig. 11. So, care should be taken about the faithfulness of EU22. This is just presented for an interesting comparison and to follow the topological changes in the latest European data. The graph dimension, measured by the breadth-first search algorithm, defined by

$$\langle N_r \rangle \sim r^d \ , \tag{11}$$

where N_r is the number of nodes that are at a topological (also called "chemical") distance r from each other, resulted in $d < 2$, unlike for the other networks, see Table 2. It is also shown that the N_r results in the inset of Fig. 7.

The EU22 is also less heterogeneous than the other networks, calculating the highest modularity with $\Gamma = 1$ results in a score of $Q_{EU22} = 0.93346$ from the contribution of only 92 communities.

The community structures of the investigated networks are summarized in Table 1. The EU16 and US16 graphs exhibit very similar structures, the same number of communities for the same resolution $\Gamma = 10^{-4}$ and their size distribution is also very similar as one can see on Fig. 8. This graph also shows the effect of Γ on the size distributions: lower Γ results in faster decays. However, the EU22 network is different both in the lower number of communities and their fast decaying distribution.

In conclusion, our results imply that

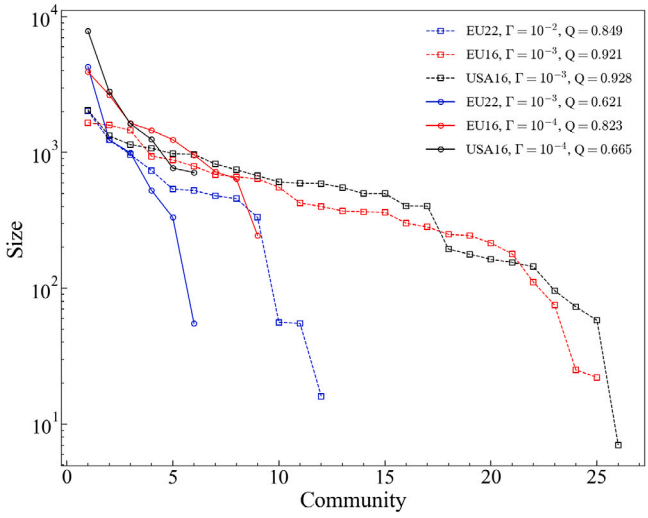

Fig. 8. Community size distributions at different Γ resolution parameters for the different networks shown in the legend.

(i) the continent sized synchronous areas exhibit similar PLs in their degree distributions,

(ii) however, sub-systems show deviations from these patterns, leading to synchronization at smaller couplings. Thus, these sub-systems are more likely to show Chimera states.

2.4. Topographical structure of the power-grids

In order to relate topological communities to the topography, the modularity scores have been calculated with a lower Γ resolution. The results are shown in Figs. 9–12. Note that the complete EU 2016 data-set (Fig. 9) and the giant components of that does not take into account only above 120 kV lines (Fig. 10). At the same Γ, 11 shows visibly different community structure, even though only around 50 nodes were removed from 13 478 nodes and the number of links were reduced to 17 749 not significantly far from 18 393. The modularity score also shows little difference. However, on the two maps, it is noticeable that the Apennine Peninsula is split into multiple smaller communities. It is also worth mentioning that when a higher threshold is introduced (e.g. lines below 220 kV are left out), the network falls completely apart. Considering "true" communities with $\Gamma = 1$, the resulting modularity score cannot get higher than $Q_{EU16-shattered} = 0.2499$ with 344 communities. In the case of the 2016 base network with removed links, was used. The community boundaries were compared to the real topology of the European power grid to identify the main topological reasons for the results.

In Fig. 9, two cut-sets are shown, the separation of the British Isles and the Iberian Peninsula from the rest of continental Europe. In the first case, the cut-set consists of three HV direct current lines, while in the second case, it is four AC lines (220 kV and 400 kV). The split in Northern Italy is along the 400 kV connection between La Spezia–Vignole–Baggio, an important north–south interconnection. The community in Southern Norway mainly consists of 330 kV lines, in contrast to the surrounding areas' 400 kV subsystems. Finally, the imprints of history (e.g. the Iron Curtain) can be recognized in Central Eastern Europe, which is separated from the Western part of the continental system, but is also distinguishable from the IPS/UPS (Integrated Power System, Unified Power System) cooperation of the former Soviet Union.

Fig. 10 shows similar results for the British Isles, the Iberian Peninsula and the separation between Central Eastern and Western Europe. A notable difference is that the cut-set between Italy and its neighboring countries is formed according to the political borders in this case. Northern and Southern parts of Italy are separated along bottlenecks

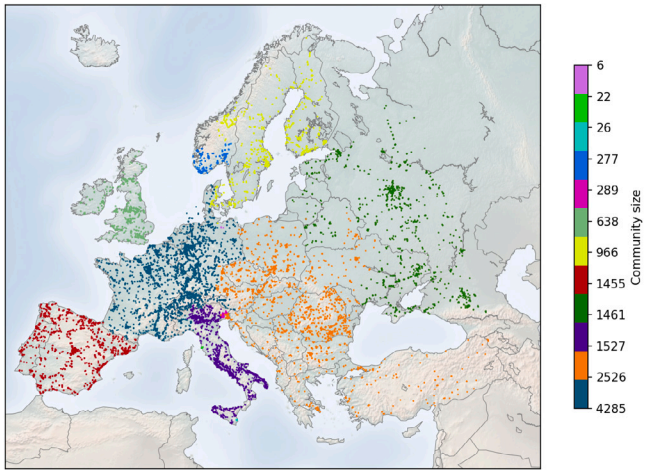

Fig. 9. All nodes of the European power-grid 2016 data separated into 12 communities, taking into account admittance, using a giant component of 13 478 nodes connected by 18 393 links, maintaining the modularity score close to the maximum $Q \approx 0.795$.

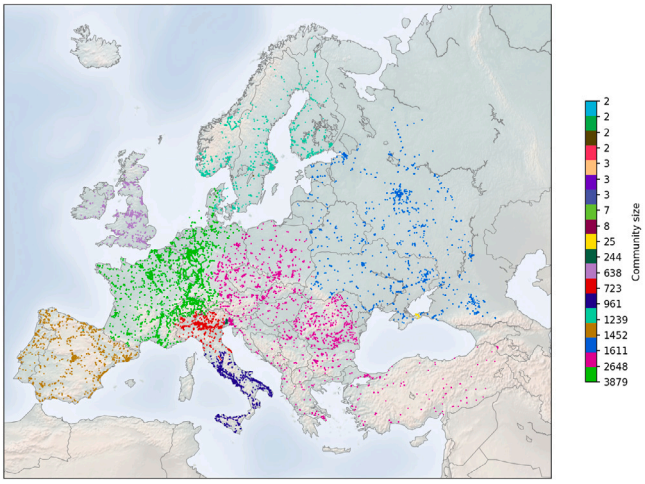

Fig. 10. Nodes of the European HV power-grid 2016 data giant component. Excluding lines below 120 kV and using $\Gamma = 10^{-4}$ resolution, taking into account the admittance values the graph is separated into 19 communities. A giant component of 13 420 nodes linked with 17 749 edges emerges, giving a modularity score at this resolution $Q \approx 0.785$.

formed by the Piombino–Poggio, Piombino–Calenzano and the Candia–Teramo 400 kV lines. The split in Denmark is along the parallel 400 kV connections between Ferslev and Jardelund. Finally, the former Soviet states are separated from the rest of Europe along the different transmission voltage levels, which is 330 kV in the former and 220 and 400 kV in the latter region.

A partially different result of community detection is seen in Fig. 11, where the effects of HV direct current lines is more emphasized. This is clearly seen (i) in the case of Ireland and Great Britain with the Auchencrosh–Ballycronanmore (the Moyle Interconnector) and Deeside–Woodland (the East–West Interconnector) lines, (ii) for the island of Sardinia with the Bonifacio–S.Teresa (SACOI) and Fiume Santo–Latina (SAPEI) lines, and (iii) in the Southern Scandinavian region with the Fraugde–Herslev (Storebælt HVDC), Bjæverskov–Bentwisch (KONTEK), Kruseberg–Herrenwyk (Baltic Cable) connections. Other easily identifiable cut-sets are seen on the western borders of Turkey (Filippi–N.Santa single and Maritsa Iztok 3–Hamitabat double 400 kV lines) and between Europe and Africa (Fardioua–Tarifa line).

As for the power grid of the USA (Fig. 12), similar telltale signs are seen. In general, the outlines of the Eastern, the Western and the Texas Interconnection can be recognized, but both large areas are divided into more sub-parts. The northern and southern parts of the Western Interconnection are divided along the cut-set of 500 kV lines. The state of Colorado lacks significant interconnections, and thus it forms a separate community. The three largest communities of the Eastern Interconnection indicate the use of different dominant transmission voltage levels, namely 345 kV in the northwestern region, and a mix of 161 , 230 and 500 kV in the remaining parts. The other three large communities (two in the US Northeast and Florida) are rather the results of their geographical properties. An interesting feature of the map is that the orange community includes both Eastern and Western parts; the backbone of this community is a 230 kV topological formation.

In conclusion the detection of communities helps in understanding the unique patterns and the heterogeneity that characterizes the topology and thus the dynamic behavior of the system. The topographical maps can also help the research community to identify those sub-systems that are suitable for the detection of Chimera states.

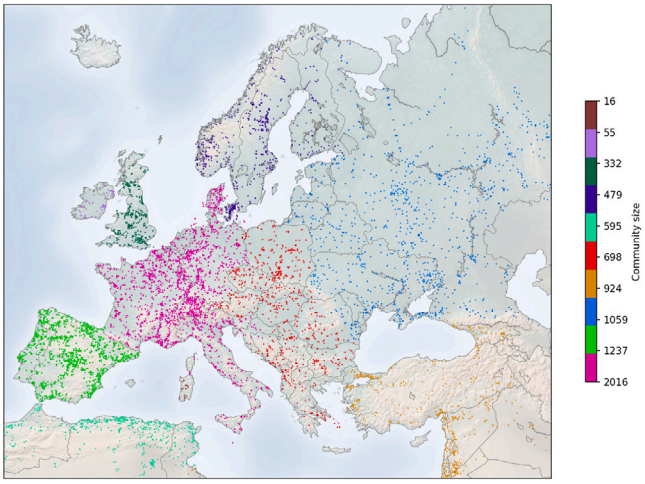

Fig. 11. All nodes of the European power-grid 2022 data giant component, separated into 10 communities, taking into account the admittances and 7411 nodes connected by 10 912 edges without smaller voltage level edges, maintaining the modularity score $Q \approx 0.854$.

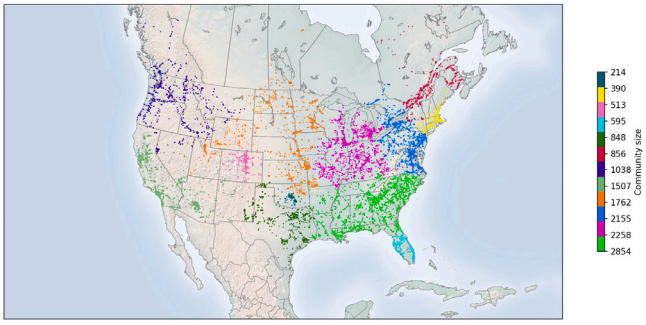

Fig. 12. All nodes of the USA power-grid 2016 data giant component, separated into 12 communities, taking into account the admittances and 14 990 nodes connected by 20 880 edges, maintaining the modularity score $Q \approx 0.859$ with resolution $\Gamma = 1 \times 10^{-4}$.

3. Numerical modeling

To further elaborate the findings of Section 2, especially in relation to the heterogeneity of network structures and the role of communities, dynamical simulations were performed. To solve the differential equations, the adaptive Bulirsch–Stoer stepper [80] was applied, which provides more precise results for large K coupling values than the fourth-order Runge–Kutta method. The solutions depend on the ω_i^0

values and become chaotic, especially at the synchronization transition. Thus, to obtain reasonable statistics, we needed strong computing resources, using parallel codes running on GPU clusters.

To obtain larger synchronization, the initial state was set to be phase synchronized: $\theta_i(0) = 0$, but due to the hysteresis one can also investigate other uniform random distributions like: $\theta_i(0) \in (0, 2\pi)$. The initial frequencies were set as: $\dot{\theta}_i(0) = \omega_i^0$.

To characterize the phase transition properties, both the phase order parameter $R(t)$ and the frequency spread $\Omega(t)$, referred to as the frequency order parameter, were studied. The Kuramoto phase order parameter was measured:

$$z(t_k) = r(t_k)\exp\left[i\theta(t_k)\right] = 1/N\sum_j \exp\left[i\theta_j(t_k)\right] \ . \tag{12}$$

Sample averages for the phases

$$R(t_k) = \langle r(t_k)\rangle \tag{13}$$

and for the variance of the frequencies

$$\Omega(t_k, N) = \langle \frac{1}{N}\sum_{j=1}^{N}(\overline{\omega}(t_k) - \omega_j(t_k))^2\rangle \tag{14}$$

were determined, where $\overline{\omega}(t_k)$ denotes the mean frequency within each respective sample. To locate the synchronization crossover points better, their variances were determined: $\sigma(R)$ and $\sigma(\Omega)$.

3.1. Modeling admittances and weights in incomplete databases

In order to carry out synchronization calculations for detailed case studies, missing admittances and graph edge weights must be estimated. One of the possible solutions is to use the physical parameters of the grid if they are known. The backbones of the EU16 and US16 networks are based on the SciGRID project [69], which relies on the 2016 statistics of ENTSO-E and data obtained from OpenStreetMap (.osm) files. The backbone of the EU22 network is based on the data from the PyPSA-Eur python package [70], which is a model and dataset of the European power system at the transmission network level. The transmission network data is based on a cleaned-up extraction of the Interactive ENTSO-E Transmission Network Map, extracted using GridKit [81]. Since acquiring data from .osm files is not always possible, the resulting data set may be incomplete. In the following a possible solution is presented to substitute the missing data.

The power grid may be interpreted as a graph, where the nodes correspond to generators (power sources) or loads (consumers). At the same time, the transmission lines may be considered the edges in the graph. First, the largest connected component of the grid was considered. Selecting the known voltage data for the links makes it possible to estimate the rest of voltages. Averaging the available voltages in the giant component yields the average voltage, $\overline{V}$ of the known links. As the simplest possible assumption, this average value was entered in the system as the voltage level for every unknown entry in the database.

This is a different approach compared to what is used typically in synthetic grid models. The original SciGRID database extracts topological data from OpenStreetMap files using an SQL script. The method proposed here, however, builds a model dominantly relying on physical properties. Drawing on our expertise in grid modeling, specific values of the relevant quantities (such as the resistance, the reactance and the capacitance) are proposed as the function of the voltage level. For the exact values used, see Table 2.

Electrical parameters could be calculated by grouping the edges in different voltage levels and performing the calculations on the common voltage level of the network. Three groups are identified in the networks, as shown in Table 2: 120 kV, 220 kV, 380 kV. The boundaries between these categories are defined as the arithmetic mean of two neighboring voltage levels. A link will have the characteristic parameters of the category it is closest to. That is, every link below 120 kV is part of the first category, having the parameters of the 120 kV lines. Every line above 380 kV is part of the 380 kV class. The category for rest of the links will be decided based on the closeness to the above-defined boundaries. Section 2.B shows that the voltage levels with the biggest population (220 kV and 380 −400 kV) represent approx. 90% of the lines.

Table 2
Characteristic values of relevant physical quantities in the modeled European power grids.

Voltage [kV]	R_c [Ω/km]	X_c [Ω/km]	C_c [nF/km]	P_c [MW]
120	0.0293	0.1964	9.4	170
220	0.0293	0.2085	9.0	360
380/400	0.0286	0.3384	10.8	1300

Having decided the voltage class of a line, the relevant quantities are computed:

$$R_{ij} = \left(\frac{U_c}{U_{ij}}\right)^2 \cdot L_{ij} \cdot R_{c_k} \tag{15}$$

$$X_{ij} = \left(\frac{U_c}{U_{ij}}\right)^2 \cdot L_{ij} \cdot X_{c_k} \tag{16}$$

$$P_{ij} = P_{c_k}, \tag{17}$$

where R_{c_k}, X_{c_k} are characteristic values belonging to level k and U_c = 220 kV is the most common level for the European grid. The weight of the link from node i to j is defined as:

$$W_{ij} = \frac{P_{ij}}{X_{ij}} \Big/ \left\langle \frac{P}{X} \right\rangle, \tag{18}$$

where P_{ij} is the nominal power of the link on its voltage level, and X_{ij} is its impedance. The normalization factor has been chosen to be the average value of this fraction calculated for the whole network.

PDFs of admittances of the European EU16 grid, and for comparison, those of the US16 North-American power-grid [69,81] have been calculated. The data was obtained by the same data completion method as described above. With this extension, in the case of the 2016 North-American network, 9527 (45%) new links were estimated. For the 2016 European and 2022 European networks, 5167 (28%) and 40 (0.3%) new links with admittances were estimated, respectively. Fig. 13 demonstrates that the US16 and EU16 grids exhibit very similar heavy tails. These can be fitted by PL-s of the form $p(Y) \propto Y^{-x}$ in the region: $10^2 < Y < 10^4$ [1/ohms], characterized by the exponents: $x_{EU16} = 2.03(3)$, $x_{US16} = 2.05(5)$.

Furthermore, a Lomax-II [82], related to Pareto distribution in the form:

$$p(Y) = \frac{A}{\Lambda}\left[1 + \frac{Y}{\Lambda}\right]^{-(A+1)}, \qquad Y \geq 0, \tag{19}$$

can describe even the low Y range, with a high goodness factor: R^2 = 0.987 for EU16, and R^2 = 0.994 for US16 as shown in the inset of Fig. 13. However, in case of the EU22 data, a different behavior is detected in the intermediate Y range. This is probably the consequence of the incomplete data-set. We have not tried to apply a numerical tail fit.

These heavy tails of lines with larger admittances are the consequence of very short edge lengths in the databases, which can take values of a few meters. In the case of the EU22 data-set, the same behavior was not identified. The reason might be that it does not contain all HV links. The incompleteness of the EU22 graph is obvious, because it contains only 10298 edges, as compered to the EU16 case, which has 18393 edges. This is so, even though the EU22 grid includes territories of North Africa and the Middle East as well, see Fig. 11.

To investigate this further, the cable lengths of the 2016 SciGRID data bases were analyzed. Fig. 14 shows the PDF-s of $l_{\max}/l$, which would be proportional to the admittances if cables were uniform with the same characteristic resistances. The distributions are very similar. But the tails break down more rapidly than for the admittance distributions, suggesting a stretched exponential. The right inset, showing the PDF of lengths in meters, exhibits larger curvatures on the log–log plot.

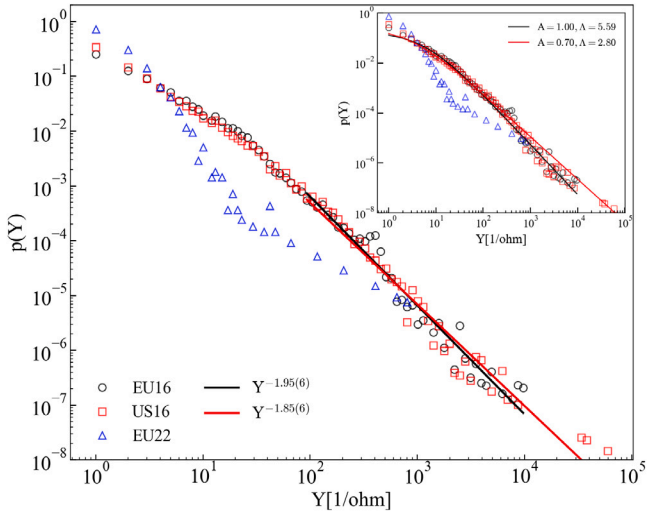

Fig. 13. Probability distributions of the calculated admittances of the 2016 European (bullets), North-American (boxes) SciGRID and the 2022 EU (stars) networks. Dashed line: least squares PL fit to the EU16, dotted line: for the US16, in the region: [100..10000] 1/ohm. The inset shows the same data, fitted with the form Eq. (19), which works well down to the 10 [1/ohm] region.

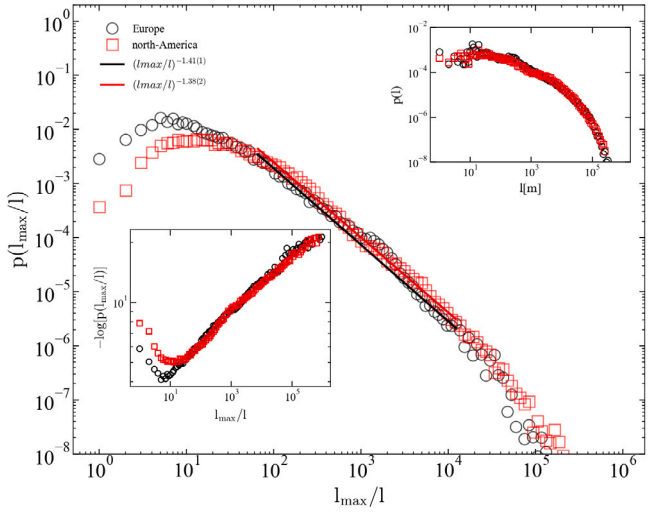

Fig. 14. Probability distributions of the inverse of cable lengths of the European and North-American SciGRID networks. Left inset: the same data plotted on the $-\ln(p)$ scale to compare with the stretched exponential assumption that would correspond to a straight line tail. Right inset: probability distributions of the line lengths in meters.

3.2. Frustrated synchronization, Chimeras in modules of the European power-grid

Heterogeneity is known to cause so-called frustrated synchronization [34,36], such that for a given control parameter set certain domains exhibit (at least partial) synchronization, while others do not. This is also related to the so-called Chimera states [38,83], in which subsets of an ensemble of identical, interacting oscillators exhibit distinct dynamical states: such as a group of synchronized oscillators and a group of desynchronized ones [84]. First chimeras were defined in systems of identical oscillators [84,85]. In this case, a non-zero phase lag term is essential for partial synchronization to occur. Realistic models, however, require oscillators to be heterogeneous and chimera-like states have also been reported in complex networks [83,86–88], in human [89–91], as well as in C-elegans [92] neural networks. By focusing on power-system networks, this study follows the second line of chimera definition for heterogeneous systems.

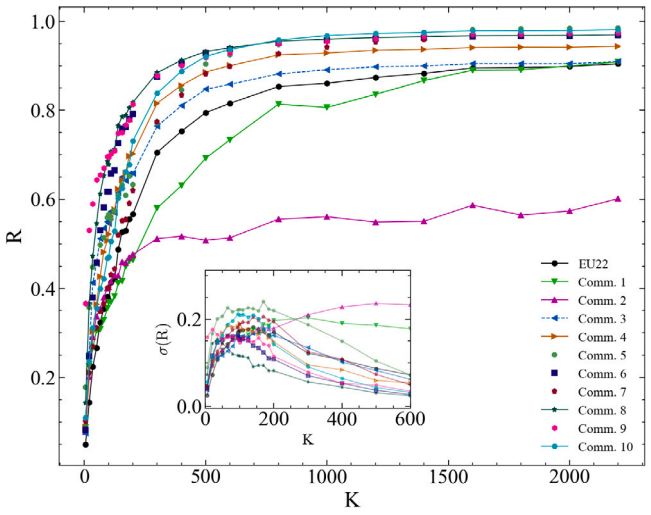

Fig. 15. Community dependence of R for different K-s at $\alpha = 0.4$ in the EU22 network shows different phase synchronizations, corresponding to "Chimera" states. The thick black curve denotes the synchronization of the whole system, which grows the slowest by increasing K. Inset: Fluctuations of the same data, showing different synchronization points. The thick black curve, representing the whole system does not exhibit the rightmost peak, as for the EU16 power-grid [91], instead the community 2, corresponding to the Nordic power-grid.

The main criterion to call partially synchronized states as chimera-like stated in [87] is "the coexistence of coherent and incoherent domains in space". The second significant feature of chimera-like states is the difference of averaged oscillator frequencies. Usually, the oscillators belonging to the coherent domains have identical frequencies; while oscillators from incoherent domains are characterized by higher or lower mean frequencies.

To show the appearance of this phenomenon, we calculate $R(t \to \infty)$ and the variance $\sigma(R)$ in the communities determined before. In the first step, $i = 1, \ldots, 12$ community decomposition was used and $R_i(t \to \infty)$ was determined. Then it was averaged over the numerical solution of 100 independent self-frequency samples and for $1200 < t \leq t_{\max} = 2000$ time steps in the steady state, following an initialization from fully phase synchronized states. As Fig. 15 shows, $R_i(t \to \infty)$ values increase as the value of K grows in a different way in different communities. The curves exhibit distinct fluctuation peaks, shown in the inset. That means for a given K, some communities are synchronized at least partially, while others are not. Note that in the EU16 network, for the communities $3, 6, 7$ the Kuramoto order-parameter remains close to 1, and there is no peak in $\sigma(R)$ [91]. This is a consequence of having only a small number of nodes within the communities (see Table 2), which shows synchronization for very small Ks.

On the other hand, in the case of the EU22 graph, communities 1, 2 synchronize at higher K-s than the whole system. Therefore, the simple size dependence law, which is valid for independent finite graphs [93], does not seem to hold. But non-trivial topological features of the EU22 graph cause that the Turkish and the Nordic region are less synchronized for a given K. This has also been found to be true with a larger damping factor $\alpha = 3$ in the solution of the Kuramoto equation.

In the case of disordered initial conditions, the fluctuation peaks shift to the right with respect to the above results. Also, the steady state values are lower than those of the global order parameter, which exhibits a hysteresis and meta-stable states near the crossover point [25].

Similar results were found for the frequency spread order parameter Ω, without a peak in the variances $\sigma(\Omega)$ as in previous publications [25, 93].

Table 3
Summary of fitted data for the power grids. d denotes the graph dimension (11), Q (at different Γ values) is the modularity quotient (10), $\langle k \rangle$ is the average degree, γ is the decay exponent of the exponential of the degree distribution (9), β is the power capacitance exponent of the generators (8), x is the admittance decay exponent.

Network	d	Q (1)	Q (10^{-4})	$\langle k \rangle$	γ	β	x
USNW	2.3(1)	0.929	–	2.67	0.55	–	–
EU16	2.6(1)	0.927	0.829	2.729	0.49	0.25	2.03(3)
US16	2.4(1)	0.925	0.734	2.785	0.49	0.25	2.05(5)
EU22	1.8(2)	0.933	0.693	2.779	0.56	–	–

4. Discussion

In summary, similar graph and electrical characteristics were obtained for the North American and European power-grids. The relevant graph dimensions are: d, modularity: Q, average degree: $\langle k \rangle$, coefficient of the exponential degree form: γ, capacitance stretched exponent of the generators: β, and the PL exponent of cable admittances: x as summarized in Table 3. The agreement is remarkable, although the EU22 values are a bit off, due to the incomplete data-set. These findings strengthen the hypothesis that both continent-sized power grids will behave similarly, when studying their stability.

There is an interesting deviation in the community level synchronization behavior of EU22 from the EU16 [91] results and expectations, based on synchronization of the second order Kuramoto model on lattices. Namely, the Turkish and Nordic communities synchronize at higher global couplings than the whole system, in contrast with expectations by the synchronization crossover size dependence of independent, lattice systems [93]. This is related to the special topological connections of these regions in the EU22 power-grid network. It also strengthens the necessity to simulate power-grids carefully, by checking approximations in the interactions.

Besides, a good agreement was found between the frequency fluctuation analysis of the Hungarian MAVIR data $q \simeq 1.1$ (entropic index) and the results for the Nordic power-grid see Ref. [51].

The above discussed findings confirm that (i) heterogeneity of the models is substantial to create realistic dynamical simulations, and that (ii) the size of the grid under study does affect the outcomes of these simulations, despite the existence of underlying universalities.

5. Conclusions

This study described the detailed analysis of the European and North American power-grids on the network topological and topographical level. In addition, the dynamical solution of the swing equation was provided. It was shown that when having augmented databases, weights could be assigned to capacities to emulate the heterogeneity of real networks. These weights could be fed as additional input into the simulations. This represents an important enhancement compared to previous results, where only the network's topology was considered [25].

The similarities in the graph topological electrical measures between the power-grids of the two continents, especially the cable length distributions, suggest a universality hypothesis. It breaks down as we go towards the lower level sub-systems or as the consequence of undersampling, like subsets of real data. The latter can very well be observed for the obviously incomplete EU22 power-grid case, which provides results resembling smaller regions. An example is the USNW, corresponding to the North-West states of the US. In general, universality is expected to occur in the infinite system size limit, according to statistical physics [94] and the behavior in smaller systems can deviate from it. Our extensive, continent-sized analysis provides an opportunity to observe this phenomenon.

Our non-perturbative analysis goes beyond linear approximations or DC models. It reflects a non-trivial relation of heterogeneity and synchronization stability. Community structure decomposition, followed by the solution of equations of motion, do not only reveal frustrated synchronization patterns, but also the non-trivial topological effects on the synchronization stability.

A frequency fluctuation analysis of Hungarian data was also presented. These fluctuations can be described by similar super-statistics and q exponent, as the ones published for the Nordic grid region [59, 60]. This finding also strengthens the universality hypothesis we advance in this paper.

While the findings of this study reveal the importance of properly modeling the heterogeneity of grid parameters, it is also debated (e.g. in [95]), whether the previously introduced order parameters capture all transitions. In our ongoing studies we extend the details of the models presented in this paper to reveal the shortcomings of various order parameters

Our future work will focus on the extension of the Kuramoto model with the amplitude of nodal voltages, which would allow a more accurate calculation in case of networks consisting of multiple voltage levels. We expect this development to open up new research questions, e.g. the involvement of LV distribution networks, the analysis of hybrid AC–DC systems and the search for network bottlenecks (i.e. Braess' paradox).

CRediT authorship contribution statement

Bálint Hartmann: Writing – original draft, Visualization, Validation, Supervision, Resources, Project administration, Methodology, Investigation, Funding acquisition, Formal analysis, Conceptualization. **Géza Ódor:** Visualization, Validation, Supervision, Software, Resources, Project administration, Methodology, Funding acquisition, Formal analysis, Data curation, Conceptualization. **István Papp:** Writing – original draft, Visualization, Software, Investigation, Formal analysis, Data curation. **Kristóf Benedek:** Investigation. **Shengfeng Deng:** Writing – original draft, Visualization, Software, Investigation, Formal analysis, Data curation. **Jeffrey Kelling:** Writing – original draft, Validation, Software.

Declaration of competing interest

The authors declare the following financial interests/personal relationships which may be considered as potential competing interests: Balint Hartmann reports financial support was provided by ELKH-Eotvos Lorant Research Network. Geza Odor reports financial support was provided by National Research Development and Innovation Office. If there are other authors, they declare that they have no known competing financial interests or personal relationships that could have appeared to influence the work reported in this paper.

Data availability

Data will be made available on request.

Acknowledgments

Support from the Hungarian National Research, Development and Innovation Office NKFIH (K146736) and from the ELKH grant SA-44/2021 is acknowledged. Bálint Hartmann acknowledges the support of the Bolyai János Research Scholarship of the Hungarian Academy of Sciences. We thank for the access of the Hungarian supercomputers via KIFU.

References

[1] G. Filatrella, A.H. Nielsen, N.F. Pedersen, Analysis of a power grid using a Kuramoto-like model, Eur. Phys. J. B 61 (4) (2008) 485–491.
[2] F. Dörfler, F. Bullo, Synchronization and transient stability in power networks and nonuniform Kuramoto oscillators, SIAM J. Control Optim. 50 (3) (2012) 1616–1642.
[3] F. Dörfler, F. Bullo, Synchronization in complex networks of phase oscillators: A survey, Automatica 50 (6) (2014) 1539–1564.
[4] S. Olmi, A. Navas, S. Boccaletti, A. Torcini, Hysteretic transitions in the Kuramoto model with inertia, Phys. Rev. E 90 (4) (2014) 042905.
[5] Y. Kuramoto, Self-entrainment of a population of coupled non-linear oscillators, in: H. Araki (Ed.), in: Mathematical Problems in Theoretical Physics, vol. 39, 1975, pp. 420–422.
[6] F.A. Rodrigues, T.K.D. Peron, P. Ji, J. Kurths, The Kuramoto model in complex networks, Phys. Rep. 610 (2016) 1–98.
[7] G. Ódor, B. Hartmann, Power-law distributions of dynamic cascade failures in power-grid models, Entropy 22 (6) (2020) 666.
[8] R. Albert, I. Albert, G.L. Nakarado, Structural vulnerability of the North American power grid, Phys. Rev. E 69 (2004) 025103.
[9] B.A. Carreras, D.E. Newman, I. Dobson, A. Poole, Initial evidence for self-organized criticality in electric power system blackouts, in: Proceedings of the 33rd Annual Hawaii International Conference on System Sciences, IEEE, 2000, pp. 6–pp.
[10] P. Bak, C. Tang, K. Wiesenfeld, Self-organized criticality: An explanation of the 1/f noise, Phys. Rev. Lett. 59 (1987) 381–384.
[11] I. Dobson, B.A. Carreras, V.E. Lynch, D.E. Newman, Complex systems analysis of series of blackouts: Cascading failure, critical points, and self-organization, Chaos 17 (2) (2007) 026103.
[12] B. Carreras, D. Newman, I. Dobson, A. Poole, Evidence for self-organized criticality in a time series of electric power system blackouts, IEEE Trans. Circuits Syst. I. Regul. Pap. 51 (9) (2004) 1733–1740.
[13] T. Nesti, F. Sloothaak, B. Zwart, Emergence of scale-free blackout sizes in power grids, Phys. Rev. Lett. 125 (5) (2020) 058301.
[14] C. Duan, T. Nishikawa, A.E. Motter, Prevalence and scalable control of localized networks, Proc. Natl. Acad. Sci. 119 (32) (2022) http://dx.doi.org/10.1073/pnas.2122566119.
[15] Y. Yang, T. Nishikawa, A.E. Motter, Small vulnerable sets determine large network cascades in power grids, Science 358 (6365) (2017) http://dx.doi.org/10.1126/science.aan3184.
[16] Y. Yang, T. Nishikawa, A.E. Motter, Vulnerability and cosusceptibility determine the size of network cascades, Phys. Rev. Lett. 118 (4) (2017) http://dx.doi.org/10.1103/physrevlett.118.048301.
[17] Y. Yang, A.E. Motter, Cascading failures as continuous phase-space transitions, Phys. Rev. Lett. 119 (24) (2017) http://dx.doi.org/10.1103/physrevlett.119.248302.
[18] Y. Yang, J. Wang, A.E. Motter, Network observability transitions, Phys. Rev. Lett. 109 (25) (2012) http://dx.doi.org/10.1103/physrevlett.109.258701.
[19] B. Schäfer, D. Witthaut, M. Timme, V. Latora, Dynamically induced cascading failures in power grids, Nature Commun. 9 (1) (2018) 1–13.
[20] F. Molnar, T. Nishikawa, A.E. Motter, Network experiment demonstrates converse symmetry breaking, Nat. Phys. 16 (3) (2020) 351–356.
[21] P. Jaros, R. Levchenko, T. Kapitaniak, J. Kurths, Y. Maistrenko, Asymmetry induces critical desynchronization of power grids, Chaos 33 (1) (2023) 011104, arXiv:https://pubs.aip.org/aip/cha/article-pdf/doi/10.1063/5.0131931/16756782/011104_1_online.pdf.
[22] G. Ódor, B. Hartmann, Heterogeneity effects in power grid network models, Phys. Rev. E 98 (2) (2018) 022305.
[23] G. Ódor, B. Hartmann, Power-law distributions of dynamic cascade failures in power-grid models, Entropy 22 (6) (2020) 666.
[24] A.E. Motter, C. Zhou, J. Kurths, Network synchronization, diffusion, and the paradox of heterogeneity, Phys. Rev. E 71 (2005) 016116, URL https://link.aps.org/doi/10.1103/PhysRevE.71.016116.
[25] G. Ódor, S. Deng, B. Hartmann, J. Kelling, Synchronization dynamics on power grids in Europe and the United States, Phys. Rev. E 106 (2022) 034311, URL https://link.aps.org/doi/10.1103/PhysRevE.106.034311.
[26] B. Hartmann, S. Deng, G. Ódor, J. Kelling, Revisiting and modeling power-law distributions in empirical outage data of power systems, PRX Energy 2 (3) (2023) 033007.
[27] G. Pruessner, Self-organised criticality: Theory, models and characterisation, 2012, pp. 1–494.
[28] D. Witthaut, F. Hellmann, J. Kurths, S. Kettemann, H. Meyer-Ortmanns, M. Timme, Collective nonlinear dynamics and self-organization in decentralized power grids, Rev. Modern Phys. 94 (1) (2022) 015005.
[29] M. Rosas Casals, B. Corominas Murtra, Assessing European power grid reliability by means of topological measures, WIT Trans. Ecol. Environ. 121 (2009) 527–537.
[30] G.d.C. Martins, F. Ribeiro, L.S. Oliveira, F.L. Forgerini, Complex network analysis of the Brazilian power grid, Scientia Plena 14 (10) (2018) http://dx.doi.org/10.14808/sci.plena.2018.104802.
[31] R.B. Griffiths, Nonanalytic behavior above the critical point in a random ising ferromagnet, Phys. Rev. Lett. 23 (1) (1969) 17–19.
[32] T. Vojta, Rare region effects at classical, quantum and nonequilibrium phase transitions, J. Phys. A 39 (22) (2006) R143.
[33] G. Ódor, R. Dickman, G. Ódor, Griffiths phases and localization in hierarchical modular networks, Sci. Rep. 5 (2015) 14451.
[34] P. Villegas, P. Moretti, M.A. Munoz, Frustrated hierarchical synchronization and emergent complexity in the human connectome network, Sci. Rep. 4 (1) (2014) 1–7.
[35] P. Villegas, J. Hidalgo, P. Moretti, M.A. Muñoz, Complex synchronization patterns in the human connectome network, in: Proceedings of ECCS 2014, Springer, 2016, pp. 69–80.
[36] A.P. Millán, J.J. Torres, G. Bianconi, Complex network geometry and frustrated synchronization, Sci. Rep. 8 (1) (2018) 1–10.
[37] G. Ódor, M.T. Gastner, J. Kelling, G. Deco, Modelling on the very large-scale connectome, J. Phys: Complexity 2 (4) (2021) 045002.
[38] D.M. Abrams, S.H. Strogatz, Chimera states for coupled oscillators, Phys. Rev. Lett. 93 (2004) 174102.
[39] G. Ódor, G. Deco, J. Kelling, Differences in the critical dynamics underlying the human and fruit-fly connectome, Phys. Rev. Res. 4 (2022) 023057.
[40] J. Grainger, D. Stevenson, Power system analysis, McGraw-Hill, 1994.
[41] Y. Guo, D. Zhang, Z. Li, Q. Wang, D. Yu, Overviews on the applications of the kuramoto model in modern power system analysis, Int. J. Electr. Power Energy Syst. 129 (2021) 106804.
[42] H. Taher, S. Olmi, E. Schöll, Enhancing power grid synchronization and stability through time-delayed feedback control, Phys. Rev. E 100 (6) (2019) 062306.
[43] B. Schäfer, C. Beck, K. Aihara, D. Witthaut, M. Timme, Non-Gaussian power grid frequency fluctuations characterized by Lévy-stable laws and superstatistics, Nat. Energy 3 (2) (2018) 119–126.
[44] G. Filatrella, A.H. Nielsen, N.F. Pedersen, Analysis of a power grid using a Kuramoto-like model, Eur. Phys. J. B 61 (2008) 485–491.
[45] S. Olmi, A. Navas, S. Boccaletti, A. Torcini, Hysteretic transitions in the Kuramoto model with inertia, Phys. Rev. E 90 (4) (2014) 042905.
[46] R.S. Pinto, A. Saa, Synchrony-optimized networks of Kuramoto oscillators with inertia, Phys. A 463 (2016) 77–87.
[47] H. Taher, S. Olmi, E. Schöll, Enhancing power grid synchronization and stability through time-delayed feedback control, Phys. Rev. E 100 (6) (2019) 062306.
[48] G. Ódor, B. Hartmann, Heterogeneity effects in power grid network models, Phys. Rev. E 98 (2018) 022305.
[49] M.F. Wolff, K. Schmietendorf, P.G. Lind, O. Kamps, J. Peinke, P. Maass, Heterogeneities in electricity grids strongly enhance non-Gaussian features of frequency fluctuations under stochastic power input, Chaos 29 (10) (2019).
[50] L. Rydin Gorjão, R. Jumar, H. Maass, V. Hagenmeyer, G.C. Yalcin, J. Kruse, M. Timme, C. Beck, D. Witthaut, B. Schäfer, Open database analysis of scaling and spatio-temporal properties of power grid frequencies, Nat. Commun. 11 (1) (2020) 6362.
[51] L.R. Gorjão, B. Schäfer, D. Witthaut, C. Beck, Spatio-temporal complexity of power-grid frequency fluctuations, New J. Phys. 23 (7) (2021) 073016.
[52] M. Anvari, L.R. Gorjão, M. Timme, D. Witthaut, B. Schäfer, H. Kantz, Stochastic properties of the frequency dynamics in real and synthetic power grids, Phys. Rev. Res. 2 (1) (2020) 013339.
[53] U. Oberhofer, L.R. Gorjão, G.C. Yalcin, O. Kamps, V. Hagenmeyer, B. Schäfer, Non-linear, bivariate stochastic modelling of power-grid frequency applied to islands, 2023, arXiv preprint arXiv:2301.04551.
[54] D. Kraljic, Towards realistic statistical models of the grid frequency, IEEE Trans. Power Syst. 38 (1) (2022) 256–266.
[55] P. Jacquod, M. Tyloo, Propagation of non-Gaussian voltage angle fluctuations in high-voltage power grids, IFAC-PapersOnLine 55 (13) (2022) 67–72.
[56] M. Tyloo, J. Hindes, P. Jacquod, Finite-time correlations boost large voltage angle fluctuations in electric power grids, J. Phys.: Complexity 4 (1) (2023) 015006.
[57] HV frequencies in Hungary within 24 hours on oct. 23 2022, 2022, Wide Area Measurement System data provided by MAVIR Hungarian TSO.
[58] S. Umarov, C. Tsallis, S. Steinberg, On aq-central limit theorem consistent with nonextensive statistical mechanics, Milan J. Math. 76 (1) (2008) 307–328.
[59] L.R. Gorjão, L. Vanfretti, D. Witthaut, C. Beck, B. Schäfer, Phase and amplitude synchronization in power-grid frequency fluctuations in the nordic grid, IEEE Access 10 (2022) 18065–18073.
[60] L.R. Gorjão, B. Schäfer, D. Witthaut, C. Beck, Spatio-temporal complexity of power-grid frequency fluctuations, New J. Phys. 23 (7) (2021) 073016.
[61] R. Tabar, Analysis and data-based reconstruction of complex nonlinear dynamical systems, vol. 730, Springer, 2019.
[62] C. Beck, E.G. Cohen, Superstatistics, Phys. A 322 (2003) 267–275.
[63] P.J. Menck, J. Heitzig, J. Kurths, H. Joachim Schellnhuber, How dead ends undermine power grid stability, Nat. Commun. 5 (1) (2014) 3969.
[64] B. Schäfer, G.C. Yalcin, Dynamical modeling of cascading failures in the Turkish power grid, Chaos 29 (9) (2019).
[65] T. Nishikawa, A.E. Motter, Comparative analysis of existing models for power-grid synchronization, New J. Phys. 17 (1) (2015) 015012.
[66] H. Kim, M.J. Lee, S.H. Lee, S.-W. Son, On structural and dynamical factors determining the integrated basin instability of power-grid nodes, Chaos 29 (10) (2019).

[67] H. Kim, How modular structure determines operational resilience of power grids, New J. Phys. 23 (6) (2021) 063029.
[68] Y. Xu, N. Myhrvold, D. Sivam, K. Mueller, D.J. Olsen, B. Xia, D. Livengood, V. Hunt, B.R. d'Orfeuil, D. Muldrew, M. Ondreicka, M. Bettilyon, U.S. Test System with High Spatial and Temporal Resolution for Renewable Integration Studies, Zenodo, 2021.
[69] C. Matke, W. Medjroubi, D. Kleinhans, SciGRID - An open source reference model for the European transmission network (v0.2), 2016.
[70] J. Hoersch, F. Hofmann, D. Schlachtberger, T. Brown, PyPSA-Eur: An open optimisation model of the European transmission system, Energy Strategy Rev. 22 (2018) 207–215, arXiv:1806.01613.
[71] US power grid, 1998, http://konect.cc/networks/.
[72] B. Hartmann, V. Sugár, Searching for small-world and scale-free behaviour in long-term historical data of a real-world power grid, Sci. Rep. 11 (1) (2021) 6575.
[73] R. Albert, A.-L. Barabási, Statistical mechanics of complex networks, Rev. Modern Phys. 74 (2002) 47–97.
[74] S. Fortunato, Community detection in graphs, Phys. Rep. 486 (3) (2010) 75–174.
[75] D. Deritei, Z.I. Lázár, I. Papp, F. Járai-Szabó, R. Sumi, L. Varga, E.R. Regan, M. Ercsey-Ravasz, Community detection by graph Voronoi diagrams, New J. Phys. 16 (6) (2014) 063007.
[76] G. Ódor, S. Deng, Synchronization transition of the second-order Kuramoto model on Lattices, Entropy 25 (1) (2023).
[77] V.D. Blondel, J.-L. Guillaume, R. Lambiotte, E. Lefebvre, Fast unfolding of communities in large networks, J. Stat. Mech. Theory Exp. 2008 (10) (2008) P10008.
[78] V.A. Traag, L. Waltman, N.J. van Eck, From Louvain to Leiden: guaranteeing well-connected communities, Sci. Rep. 9 (1) (2019) 5233.
[79] M. Newman, Modularity and community structure in networks, Proc. Natl. Acad. Sci. 103 (23) (2006) 8577–8582, arXiv:https://www.pnas.org/doi/pdf/10.1073/pnas.0601602103.
[80] K. Ahnert, M. Mulansky, Boost::odeint.
[81] B. Wiegmans, GridKit: European and North-American extracts, Zenodo, 2016.
[82] K.S. Lomax, Business failures: Another example of the analysis of failure data, J. Amer. Statist. Assoc. 49 (268) (1954) 847–852.
[83] A. Zakharova, Chimera patterns in networks: Interplay between dynamics, structure, noise, and delay, Understanding Complex Systems, Springer International Publishing, 2021.
[84] D.M. Abrams, S.H. Strogatz, Chimera states for coupled oscillators, Phys. Rev. Lett. 93 (2004) 174102.
[85] D.M. Abrams, R. Mirollo, S.H. Strogatz, D.A. Wiley, Solvable model for Chimera states of coupled oscillators, Phys. Rev. Lett. 101 (2008) 084103.
[86] Y. Zhu, Z. Zheng, J. Yang, Chimera states on complex networks, Phys. Rev. E 89 (2014) 022914.
[87] E. Schöll, Synchronization patterns and chimera states in complex networks: Interplay of topology and dynamics, Eur. Phys. J. Spec. Top. 225 (6) (2016) 891–919.
[88] J. Sawicki, I. Omelchenko, A. Zakharova, E. Schöll, Chimera states in complex networks: interplay of fractal topology and delay, Eur. Phys. J. Spec. Top. 226 (9) (2017) 1883–1892.
[89] T. Chouzouris, I. Omelchenko, A. Zakharova, J. Hlinka, P. Jiruska, E. Schöll, Chimera states in brain networks: Empirical neural vs. modular fractal connectivity, Chaos 28 (4) (2018) 045112.
[90] R.G. Andrzejak, C. Rummel, F. Mormann, K. Schindler, All together now: Analogies between chimera state collapses and epileptic seizures, Sci. Rep. 6 (1) (2016) 23000.
[91] S. Deng, G. Ódor, Chimera states in neural networks and power systems, 2023, arXiv:2307.02216 [cond-mat.stat-mech].
[92] J. Hizanidis, N.E. Kouvaris, G. Zamora-López, A. Díaz-Guilera, C.G. Antonopoulos, Chimera-like states in modular neural networks, Sci. Rep. 6 (1) (2016) 19845.
[93] G. Ódor, S. Deng, Synchronization transition of the second-order Kuramoto model on lattices, Entropy 25 (1) (2023) 164.
[94] G. Ódor, Universality in nonequilibrium lattice systems: Theoretical foundations, World Scientific, 2008, pp. 1–276.
[95] M. Schröder, M. Timme, D. Witthaut, A universal order parameter for synchrony in networks of limit cycle oscillators, Chaos 27 (7) (2017) 073119.